Transport Processes of Water and Protons through Micropores

Xue-Dong Din and Efstathios E. Michaelides
School of Engineering, Tulane University, New Orleans, LA 70118

Molecular dynamics simulations were performed to study the movement of water molecules and protons in two pores: a small pore of radius 9.36 Å and a larger one of radius 12.24 Å. Inside the ionic solution, the wall charge densities are approximately $-0.1\ C/m^2$ and $-0.2\ C/m^2$. Water and proton distributions in the pore are affected strongly by the water content and the wall charge density. In the case of low wall charge density, if there is a sufficient number of water molecules in the pore, the protons are strongly hydrated to the water molecules and do not directly contact the wall. In the case of high wall charge density, most of the protons are attracted to the wall. Then, the wall charge and the absorbed protons together behave like a weakly charged wall. We found that the Poisson–Boltzmann theory fails to predict the proton distribution in these pores. The calculated electroosmotic drag coefficient, proton diffusion coefficient, and pore conductance are compared with the simulation results for the Nafion-117 membrane. This study suggests that if the Nafion-117 membrane is modeled as a large number of identical cylindrical pores, the effective wall charge densities in the pores will never reach the value of $-0.2\ C/m^2$.

Introduction

A number of fuel-cell systems under development use perflurosulfonic acid (PSA) membranes, because they are chemically inert, structurally durable, and support high proton conductivity. Water transport is recognized as a possible problem in these membranes. Water in the membrane is transported in two main ways: electroosmotic drag of water by protons transported from anode to cathode, and diffusion down the water concentration gradient that builds up. Because water replenishment by back diffusion alone is insufficient to balance the water transported from the anode to the cathode, membrane dehydration is caused on the anode side and flooding on the cathode side. Proton conductivity is strongly coupled to the hydration of the polymer, and therefore is vital to the management of the water content inside the fuel cell.

Experiments (Verbrugge and Hill, 1990; Fuller and Newman, 1992; Zawodzinski et al., 1991, 1993b) demonstrate that the electroosmotic drag coefficient varies in a wide range, depending on the experimental methods, acid concentrations, water content, and the type of membrane. The entry of any other cations than protons in the membrane may also result in a large increase of the electroosmotic drag (Xie and Okada, 1995). The conductivity of the membrane decreases approximately linearly with the decrease of water content. Good knowledge of these parameters is important to the practical design of the water management system in the fuel cell (Nguyen and White, 1993).

The PSA membranes have a hydrophobic backbone consisting of tetrafluoroethylene units and side chains (Yeo and McBreen, 1979; Verbrugge and Hill, 1990a) The fixed ion-sites are provided by the hydrolyzed sulfonate group. The cluster-network model (Gierke, 1977) has been proposed to explain the molecular-level transport of such membranes. According to this, the PSA membrane is described as a series of ion clusters or inverted micelles, interconnected by narrow pores. These narrow pores of about 10-Å diameter connect larger pores of about 60-Å diameter. Apparently the narrow pores dominate the ion and solvent transport characteristics (Capeci et al., 1989).

A widely used theory describes the membrane as a large number of parallel cylindrical pores of identical radii with fixed charges uniformly distributed on the pore-wall surface (Gross and Osterle, 1968; Fair and Osterle, 1971; Breslau and Miller, 1971). The Poisson–Boltzmann equation is used to

determine the ion distributions inside each capillary, under static equilibrium conditions. The resulting ionic concentration profiles are then introduced to the classic continuum expressions for the transport inside the pores by the Nernst–Planck equation (Sasidhar and Ruckenstein, 1981; Christoforou et al., 1985). Thus, the solvent is considered as an incompressible continuum with its motion governed by the Navier–Stokes equations. Near the wall, solvent orientations and ion solvations have important effects on ion distributions (Garcia et al., 1990; Bontha and Pintauro, 1994).

Very little is known about the processes at the molecular level that control salt uptake and transport in these membranes. We still lack a thorough understanding of the following subjects: (1) the accuracy of the classic continuum theories when used in a region comparable with the molecular sizes and (2) the basic principles that govern the final concentrations of solvent and ionic species in a membrane?

In this work, we use the molecular-dynamics (MD) method to simulate water molecules and protons in microscopic pores. These simulations provide us with fundamental insights as to the membrane phenomena, such as the density and concentration distributions of water and protons in the pores. The computer simulations can be used to decide if the continuum theories are still qualitatively valid in microscopic pores. These simulation results are compared with experimental measurements of Nafion-117 membranes.

Molecular-Dynamics Method

Basic equations

The essence of the MD method is to calculate the forces on each molecule/particle that are the result of its interactions with all the other molecules and the surroundings of the system. Then, by numerically solving Newton's equations of motion to determine how all the molecules in the system considered move in response to these forces, the basic equation of motion may be written as follows:

$$m_i \frac{d^2 \boldsymbol{r}_i}{dt^2} = \boldsymbol{F}_{ai} + \boldsymbol{F}_{bi} + \boldsymbol{F}_{ci} + \boldsymbol{F}_{di} \tag{1}$$

where the index i indicates the ith particle, which is one of a total of N particles and $\boldsymbol{r}_i$ is its position at time t. The right-hand side of Eq. 1 is the total force acting on the particle. $\boldsymbol{F}_{ai}$ is the intermolecular force exerted by the other particles; $\boldsymbol{F}_{bi}$ represents the boundary force; $\boldsymbol{F}_{ci}$ is an overall constraint force, for example, constant temperature; and $\boldsymbol{F}_{di}$ is the driving force.

The intermolecular potential can be further divided into short-range interactions and long-range interactions. In MD simulations, it is easy to calculate the short-range interactions, because they decrease rapidly as the intermolecular distance increases. However, the calculation of the long-range interactions is time-consuming because of the slow variation of the potential with distance. For this reason, we have developed and used the GENB method (Din, 1996; Din and Michaelides, 1997), which is a combination of the general-expansion (GE) method and the neighbor-box (NB) technique. This combination has been named the GENB method and has been applied to systems with one, two, and three periodic dimensions. Through this method, the electrostatic potentials, due to particles outside the minimum images, are calculated from a general expansion method, whose coefficients are obtained by optimization. Then the NB technique is used to speed up the computation of the interactions between particles within the minimum images of the periodic systems used. If the total number of cells (boxes) is optimally selected, the computational time of the GENB method becomes proportional to $N^{3/2}$, which represents a good improvement over other methods used.

In this work, we use structured walls, which consist of regularly arranged atoms. The wall–fluid interactions can be calculated in the same way as intermolecular forces. The force $\boldsymbol{F}_{ci}$ constrains the temperature of the system. In our simulations, we use the Nosé–Hoover thermostat (Hoover, 1991) to achieve constant temperature for the system.

Driving forces

Microscopic flows can be induced by gravity, electric forces, moving boundaries, pressure gradients, concentration gradients, or temperature gradients. Several nonequilibrium MD methods have been developed, most of them pertaining to a specific driving force. In this work we used a general constraint method to simulate microscopic flows, according to Gauss's principle of least constraint (Hoover, 1991).

When the weighted average velocity of N_k particles in the system is $\overline{V}_k$, we have the following definition for it:

$$\sum_{i=1}^{N_k} W_i V_i = N_k \overline{V_k}, \tag{2}$$

where W_i is the weight of the ith particle. Differentiating this equation yields the following expression:

$$\sum_{i=1}^{N_k} W_i \frac{dV_i}{dt} = N_k \frac{d\overline{V_k}}{dt}. \tag{3}$$

According to Gauss's principle of least constraint (Hoover, 1991), the driving force of the flow, $\boldsymbol{F}_{di}$, must satisfy the following condition:

$$\sum_{i=1}^{N_k} \boldsymbol{F}_{di} \delta \boldsymbol{F}_{di} = 0, \tag{4}$$

where $\delta \boldsymbol{F}_{di}$ is the variation of the force. When this variation of the driving force is used in the transient equation of motion of a particle (Eq. 1), we obtain the following expression for the acceleration (Hoover, 1991; Din, 1996):

$$m_i \frac{dV_i}{dt} = \boldsymbol{F}_{ai} + \boldsymbol{F}_{bi} + \boldsymbol{F}_{ci} + \boldsymbol{F}_{di} + \delta \boldsymbol{F}_{di}. \tag{5}$$

Since Eq. 3 must be satisfied by both the driving force itself and the driving force plus its variation, we obtain the following constraint:

$$\sum_{i=1}^{N_k} \frac{W_i}{m_i} \delta \boldsymbol{F}_{di} = 0, \tag{6}$$

The last equation is a constraint on the variables of Eq. 5. Hence, we can use the method of Lagrange undetermined multipliers, which pertains to constraints of functions and, hence, obtain the following expression:

$$\sum_{i=1}^{N_k} \boldsymbol{F}_{di}\delta\boldsymbol{F}_{di} + \lambda_d \sum_{i=1}^{N_k} \frac{W_i}{m_i}\delta\boldsymbol{F}_{di} = 0, \tag{7}$$

where λ_d is an undetermined vector. Because the variation $\delta\boldsymbol{F}_{di}$ is arbitrary, we obtain

$$\boldsymbol{F}_{di} = -\lambda_d \frac{W_i}{m_i}, \tag{8}$$

Substituting Eqs. 1 and 8 into Eq. 3 yields the following expression (Din and Michaelides, 1994; Din, 1996):

$$\lambda_d = \frac{1}{\sum_{j=1}^{N_k} (W_j/m_j)^2}\left[\sum_{j=1}^{N_k} \frac{W_j}{m_j}(\boldsymbol{F}_{aj} + \boldsymbol{F}_{bj} + \boldsymbol{F}_{cj}) - N_k\frac{d\overline{V}_k}{dt}\right], \tag{9}$$

Generally, in a simulation it is aimed for $\overline{V}_k$ to be equal to an ensemble average $\langle \boldsymbol{V}_k \rangle$. However, because of the fluctuations on the molecular level and friction between the wall and particles, $\overline{V}_k$ may not exactly be equal to the target value $\langle \boldsymbol{V}_k \rangle$. Hence, the term $d\overline{V}_k/dt$ in Eq. 9 is expressed by a relaxation equation, which in this case is as follows:

$$\frac{d\overline{V}_k}{dt} = \frac{\langle \boldsymbol{V}_k \rangle - \overline{V}_k(t - \Delta t)}{\Delta t}. \tag{10}$$

To obtain a desired value for $\langle \boldsymbol{V}_k \rangle$, the driving force $\boldsymbol{F}_{di}$ is calculated from Eqs. 2, 8, 9, and 10. It must be pointed out that when W_i is 1, $\langle \boldsymbol{V}_k \rangle$ is the ordinary average velocity; when W_i is the relative mass of the particle, $\langle \boldsymbol{V}_k \rangle$ is proportional to the mass flux; when W_i is the relative electric charge of the particle, $\langle \boldsymbol{V}_k \rangle$ is proportional to the electric current. Therefore, the set of equations as just developed may be easily used in systems of mixtures, such as electrolyte solutions with different species (Din, 1996).

Simulation of water molecules

We use the extended simple point charge (SPC/E) model (Berendsen et al., 1987) because of its simplicity and demonstrated reasonable results. According to the SPC/E model, the water model is a rigid, nonpolarizable, planar three-site model. The three charges coincide with the positions of the hydrogen and oxygen sites. A negative charge $q_O = -0.8476e$ (e is the electronic charge) is located at the oxygen site, and a positive charge $q_H = +0.4238e$ is placed on each of the hydrogen sites. The oxygen–hydrogen fixed separation distance is 1 Å, and the angle HOH is 109.47°. The effective pair potential in the SPC/E model consists of Coulombic interactions between all intermolecular pairs and a single Lennard–Jones interaction between other oxygen sites. The water molecules are simulated by the SHAKE procedure developed by Ryckaert et al. (1977) and Van Gunsteren and Berendsen (1977).

Physical Model

Because the MD method can only simulate a limited number of molecules/particles, we consider a relatively small section of the pore. The wall of the cylindrical pore consists of regularly arranged atoms, as shown in Figure 1. The simulation cell contains 10 rings of wall atoms, with the radius of each ring being R_w. The distance between two adjacent rings is $\sigma_w\sqrt{2}/2$, where σ_w is the diameter of each wall atom. We choose $\sigma_w = 3.2$ Å. Therefore, the length of the simulation cell in the axial direction is $L_z = 22.627$ Å. Each ring on the wall has a certain number of atoms, depending on the radius of the pore studied. The rings are placed in such a way that atoms on the surface form triangular positions. When the wall is charged, the charge is uniformly distributed on each wall atom.

Two kinds of pores have been studied: the first is a small pore with $R_w = 9.36$ Å, and the other is a larger pore with

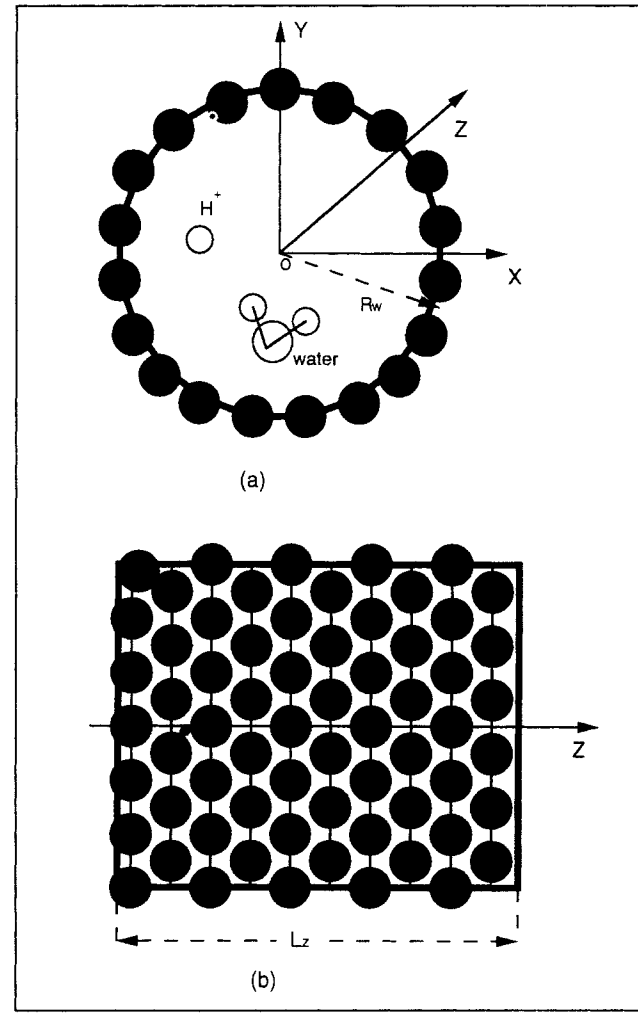

Figure 1. Cylindrical pore.

(a) cross section of the pore. (b) Wall atoms on the wall.

Table 1. Physical Parameters of Atoms

	σ(Å)	g (kcal/mol)	$q(e)$
O (Water)	3.166	0.1554	−0.8476
H (Water)	2.684	0.059	+0.4238
W (Wall)	3.2	0.101	0 ~ −0.1
H^+ (proton)	2.684	0.059	+1

σ: Diameter of the atom; ϵ: energy parameter in the Lennard-Jones potential; q: charge on the atom.

$R_w = 12.24$ Å. Because of the finite size of the atoms, the actual radius occupied by the solvent, R_0, is smaller than R_w. From the simulations we found that R_0 is about 2.02 Å smaller than R_w. For this reason, we chose $R_0 = 7.34$ Å when $R_w = 9.36$ Å, and $R_0 = 10.22$ Å when $R_w = 12.24$ Å. The reason for the choice of such narrow pores is that, according to the cluster-network model (Gierke, 1977), narrow pores of about 10–20 Å diameters dominate the transport of ions and solvents in PSA membranes.

We assume that all interactions between wall atoms and water molecules, protons, and water molecules, or wall atoms and protons are of the Lennard-Jones type added to the electrostatic (Coulombic) interactions. The sizes of the hydrogen atom and proton, the short-range interactions between water molecules and wall atoms, and the interactions between hydrogen atoms (or protons) and wall atoms are obtained from Zhu and Robinson (1991). The physical parameters of water molecules, wall atoms, and protons are summarized in Table 1.

The computer program is written and solved by the GENB method (Din, 1996). The 27-node boxes are used, and the box number is $(M_x, M_y, M_z) = (2, 2, 2)$. The temperature in the pore is kept constant at 25°C. Table 2 shows the various cases for which simulations were performed. In cases 1 and 3, there is no macroscopic flow. In the cases 2 and 8, water molecules are forced to flow and the average macroscopic velocity per water molecule is $0.1V_0$, where V_0 (= 509.2 m/s) is the characteristic velocity of the molecular simulation. In the rest of the cases, protons are forced to flow with an average macroscopic velocity equal to $0.1V_0$.

The flow velocity in our simulations is 50.9 m/s. This velocity is considerably higher than typical velocities in practical membrane applications, which are close to 1 m/s. The reason for the choice of such a high velocity for the simulations is that it results in an acceptably high signal-to-noise ratio. We think that the thermal motion of the molecules and ions is the most significant factor for the determination of the radial distribution of water molecules and protons. For this reason, we believe that the higher velocity used in the simulations does not affect this radial distribution. This was confirmed by the average results of a numerical test with low velocity, which had low signal-to-noise ratio. Of course, the magnitude of the velocity will have an effect on the hydrodynamic variables, such as the drag coefficient and the stresses on the wall.

Table 2. System Parameters

Case	R_w(Å)	N_{water}	N_+	N_{wall}	q_w(C/m^2)	$\overline{V_{av}}/V_0$	$\overline{C_+}$(M)
1	9.36	96	0	130	0	0	0
2	9.36	96	0	130	0	0.1 (water)	0
3	9.36	87	9	180	−0.1083	0	3.90
4	9.36	87	9	180	−0.1083	0.1 (ion)	3.90
5	9.36	110	9	180	−0.1083	0.1 (ion)	3.90
6	9.36	87	17	180	−0.2046	0.1 (ion)	7.37
7	9.36	130	17	180	−0.2046	0.1 (ion)	7.37
8	12.24	201	0	170	0	0.1 (water)	0
9	12.24	220	11	240	−0.1012	0.1 (ion)	2.46
10	12.24	240	22	240	−0.2024	0.1 (ion)	4.92

N_{water}: water molecule number; N_+: proton number; N_{wall}: wall atom number; q_w: wall charge density $\overline{V_{av}}$: average velocity per molecule; $\overline{C_+}$: average concentration of protons, $\overline{C_+} = N_+/\forall$, where the actual volume occupied by the solvent is $\forall = BR_0^2 L_z$; V_0: the characteristic velocity of simulations, $V_0 = 509.2$ m/s.

In cases 1, 2 and 8, there are only water molecules in the pores. The wall atoms consist of 10 rings, each having 13 atoms for the small pore and 17 atoms for the larger pore. Thus, the distribution of the wall atoms is close to that of a solid face-centered cubic (fcc) lattice. The average density of water molecules in the pores is close to that of the bulk water. The time step is $\delta t = 2$ fs. In order to avoid dependence of the averaged quantities on the initial condition of the molecules, we discarded the results of the first 100,000 steps in the computations and collected all pertinent data from the next 400,000 steps.

When the wall of the pores is negatively charged, the wall charge density is approximately −0.1 or −0.2 C/m^2. We do not consider anions in the solution, because their concentrations are generally very low inside the pores. The number of protons is chosen so that the electric neutrality condition is satisfied inside every pore. Due to the smaller size of the protons, more wall atoms must be placed on the rings to prevent the escape of protons from the pores. Therefore, each ring of the small pore has 18 wall atoms, and each ring of the larger pore has 24 wall atoms. Regarding the number of wall atoms in the different simulations, it must be pointed out that this would not significantly affect the calculations, because the interactions between the water molecules and the wall are relatively weak in comparison to the interactions between the water molecules and protons or the water molecules themselves. However, in order to avoid ambiguities in the results, the main comparisons of this study are made between charged pores of the same size with different charge densities. In this case, pores of he same size have the same number of wall atoms.

Since the mass of a proton atom is approximately 1/16 of an oxygen atom, the protons generally move much faster than water molecules. Thus, a smaller time step, $\delta t = 1$ fs, was used in the simulations. In this case, we discarded the first 100,000 steps and then simulated 800,000 more steps for the calculation of the average values.

Water Content, Electroosmotic Drag Coefficient, Conductivity, and Diffusivity

The water content, β, is defined as the ratio of water molecules to the sulfonate groups on the wall. Since no anions are considered in the solution, the number of the sulfonate groups is equal to the number of protons in the pore. Therefore, we have

$$\beta = \frac{N_{water}}{N_+}. \tag{11}$$

The electroosmotic drag coefficient, ξ, is defined as the number of water molecules moving with each ion in the absence of a concentration gradient:

$$\xi = \frac{\bar{V}_{\text{water}} N_{\text{water}}}{\bar{V}_+ N_+}. \tag{12}$$

where $\bar{V}_{\text{water}}$ and $\bar{V}_+$ are, respectively, the average velocities of water and protons in the pore. Because the water flow is caused by the drag of protons, in typical electroosmotic flows $\bar{V}_{\text{water}}$ is generally smaller than $\bar{V}_+$. The maximum value of ξ is obtained when water moves with the same velocity as the protons, that is, ξ is equal to the water content β.

The current density in the simulated system is calculated by the following expression:

$$i = FC_+ V_+, \tag{13}$$

Hence, the total current in the pore is given by the expression:

$$I = \frac{eN_+ \overline{V_+}}{L_z}, \tag{14}$$

The average current in the pore is defined as

$$\bar{i} = \frac{I}{\pi R_0^2}. \tag{15}$$

where R_0 is the actual radius, of the space that is occupied by the water molecules.

The total driving force on the protons $\boldsymbol{F}_T$, is obtained by the summation of the components $\boldsymbol{F}_{di}$ as shown in Eq. 1. This force is related to the electric field, E, by the following equation:

$$F_T = eN_+ E, \tag{16}$$

Then, the specific conductance of the pore is equal to

$$\kappa = \frac{\bar{i}}{E}. \tag{17}$$

Given the average velocity and the electric field, the ionic mobility can be calculated by the expression:

$$u_+ = \frac{\overline{V_+}}{E}. \tag{18}$$

Hence, the diffusion coefficient of ions and the ionic mobility are related by the Nerst–Einstein equation:

$$D_+ = \frac{k_B T u_+}{e}. \tag{19}$$

In order to compare the specific conductance and the diffusion coefficient obtained from the MD simulations with the experimental measurements, it is necessary to consider the porosity and tortuosity of the pores in the practical membranes. For a pore of total length L_{pore}, and membrane thickness L_m, the tortuosity is $\tau = L_{\text{pore}}/L_m$. There are N_m pores in an area of A_m on the membrane surface, and each pore has a cross-sectional area $A_{\text{pore}} = BR_0^2$. The diffusion coefficient of the membrane, D_m, is related to the diffusion coefficient inside the pore, D_+, by the expression (Epstein, 1989):

$$D_m = \frac{\theta}{\tau^2} D_+, \tag{20}$$

where θ is the porosity of the membrane. It must be emphasized that D_+ in Eq. 20 is not the diffusion coefficient in the free solution, but that in the pore. Verbrugge and Hill (1990b) further related the porosity, θ, and the diffusion coefficient of the bisulfate ion in a free solution at infinite dilution, D^0, by the following relation:

$$D_m = BD^0, \tag{21}$$

where B is a constant. For a dilute solution, it is reasonable to assume that D^0 is close to the diffusion coefficient in the pore. Noting that the relation of Eq. 21 is generally valid for any ions, one obtains the following approximation for B:

$$\frac{\theta}{\tau^2} \approx B. \tag{22}$$

If the porosity and the constant B are known, Eq. 22 may be used to determine the tortuosity.

Because of the tortuosity of the pores, the electric field of the membrane, E_m, is related to the electric field in the pores, E, by the relation

$$E_m = \frac{L_{\text{pore}}}{L_m} E, \tag{23}$$

and the total current in the membrane, I_m, is

$$I_m = N_m I, \tag{24}$$

where I is the current in a single pore. Therefore, the conductance of the membrane, κ_m, is calculated by the expression

$$\kappa_m = \frac{I_m}{A_m E_m}, \tag{25}$$

which yields

$$\kappa_m = \left(\frac{L_m}{L_{\text{pore}}}\right)^2 \left(\frac{N_m A_{\text{pore}} L_{\text{pore}}}{A_m L_m}\right) \left(\frac{I}{A_{\text{pore}} E}\right) = \frac{\theta}{\tau^2} \kappa. \tag{26}$$

Generally, θ and τ depend on the membrane type, the external concentration, and ion species. For our calculations we chose the values $B = 1.7$ and $\theta = 0.27$ for the Nafion-117 membrane (Verbrugge & Hill, 1990b).

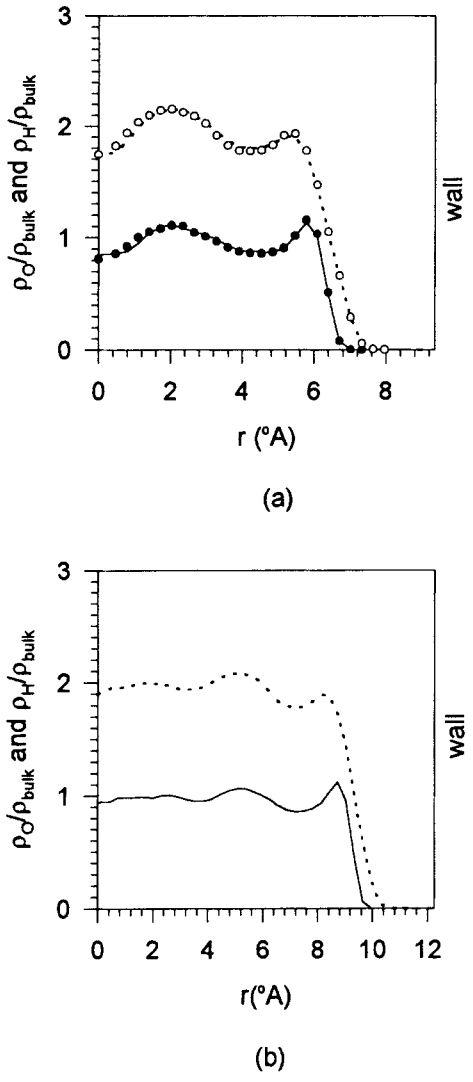

Figure 2. Pure water molecules in the pores (cases 1, 2 and 9).

$q_w = 0$. (a) In the small pore: solid line: oxygen atoms in case 1; dotted line: hydrogen atoms in case 1; solid dots and open dots: oxygen and hydrogen atoms in case 2. (b) In the large pore (case 9): solid line: oxygen atoms; dotted line: hydrogen atoms.

Results and Discussion

Pure water molecules in the pores

The density distributions of the oxygen and hydrogen atoms in the pores are shown in Figures 2a and 2b for when the pores contain only water molecules (as in the cases 1, 2, and 8 examined in this study). The wall positions indicate the centers of the wall atoms. Because of the finite sizes of the wall atoms and of the water molecules, there is no liquid in the region near the wall. It is well known that a simple fluid near the wall exhibits an oscillatory spatial distribution of its properties, and that the highest density coincides with the contact layer. Such density oscillations are indeed observed in Figure 2, but their amplitudes are not very high. It is observed that the maximum of the hydrogen density does not appear next to the wall, but closer to the center. Also that in the central region of the larger pore, the distributions are almost uniform and the water properties may be closely represented by the bulk water properties. It is evident that when water flows in the pore (case 2), the flow does not change the density distribution significantly. It must be pointed out that in these MD simulations, the structured walls are relatively smooth, and thus the flow along the walls has little effect on the density distribution in the transverse direction to the wall.

Figure 3 depicts the velocity distributions in the small and large pores. It is obvious that the velocities are affected by the statistical noise, especially in the central region. However, it is clear that the water velocities all over the pores are very close to the average velocity $0.1V_0$. Obviously, water molecules have a large slip velocity on the walls. The slip velocity is only slightly lower than the average velocity. This implies that the friction between water molecules and the walls is very small in this system. These calculated velocity profiles completely deviate from the Poiseuille theory of continuum hydrodynamics, which imposes a no-slip boundary condition and results in a parabolic velocity profile in small channels. The reason for this deviation of the velocity profile

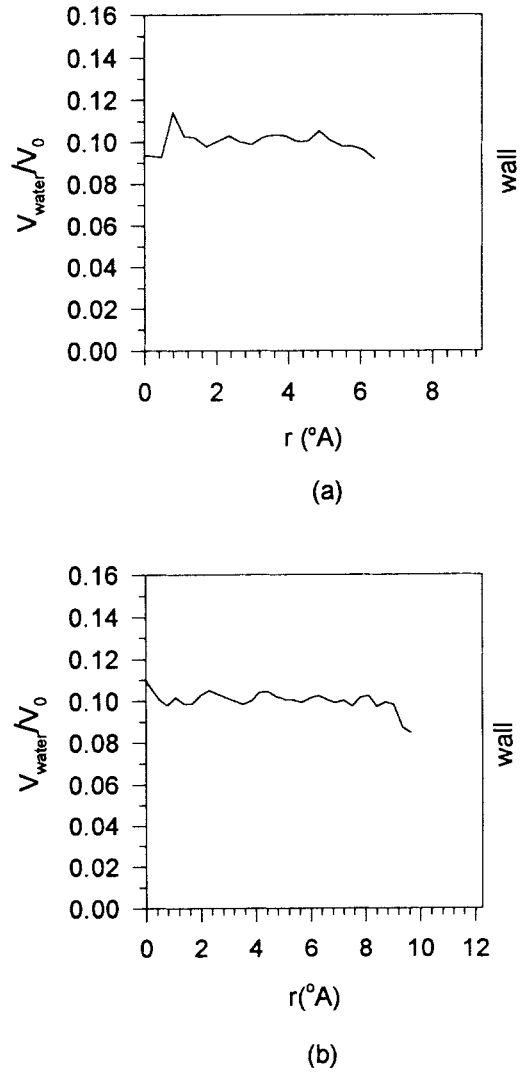

Figure 3. Water velocity distributions.

(a) In the small pore (case 2). (b) In the large pore (case 9).

from the Poiseuille theory, lies in the fact that the wall is hydrophobic. The implied weak interaction forces between the water molecules and the hydrophobic wall result in rather high slip at the wall, and consequently in a velocity profile, which is closer to plug flow. Due to the presence of the electrostatic forces, the interaction forces between the water molecules themselves are much stronger than the interaction forces between the water molecules and the wall. As a result, even the density distribution of the water molecules in the pore is very much different from the density distribution of a simple fluid in such pores, as depicted in Figure 1. Our previous simulations with simple fluids reveal that the general constraint method, which is used for the creation of a driving force in the system, yields the same results for the density and velocity distributions as other more frequently used methods (Din, 1996; Din and Michaelides, 1997). Therefore, the observed plug velocity profile is not due to the chosen method for the driving force. It must be pointed out that the main reason for the development of this method is the manifest difficulty of the introduction of a driving force in a system composed of different materials (particles/molecules/ions). A further advantage of the general constraint method is that it may be used in other complex systems, such as polymer and solvent flow.

Negatively charged pores at $q_w - 0.1$ C/m^2

Cases 3, 4, 5 and 9, correspond to a wall charge density of -0.1 C/m^2 (Table 2). In case 3 there is no macroscopic flow in the system, while in case 4 protons are forced to flow in the pore. The water and proton distributions in these two systems are shown in Figure 4. These distributions match with each other very well in most of the pore. In the central region of the pore, where very small volumes are used to collect data, larger differences are observed because of statistical noise. Therefore, one can conclude that the fluid flow has no significant effect on the distributions of electrolyte solutions in the pore.

It is apparent in Figure 4a that the water distributions are strongly influenced by the protons. The densities of the oxygen and hydrogen atoms are much higher near the wall than in the other regions. Therefore, more water molecules are dragged to the wall by the protons. The distances between the highest densities and the wall atoms are 3.27 Å for the oxygen atoms and 2.65 Å for the hydrogen atoms. The proton distribution in Figure 4b demonstrates two distinct peaks at distances 2.3 Å, and 5.1 Å from the wall, where most of the protons are located. It is observed that the first peak in the distribution of protons is closer to the wall than the highest density of the hydrogen atoms. This is due to the repulsive effect between the oxygen atoms in water molecules and the wall atoms, which affects the hydrogen atoms (attached to the oxygen atoms) but not the free protons. It is noteworthy that the second peak of the protons is higher than the first peak. This indicates that some protons are strongly attracted to water molecules, their motion is strongly affected by such water molecules, and they are thus prevented from coming in direct contact and being adsorbed by the wall. This type of proton is referred to as hydrated protons.

In case 5, more water molecules are present in the pore. The highest densities of the oxygen and hydrogen atoms are

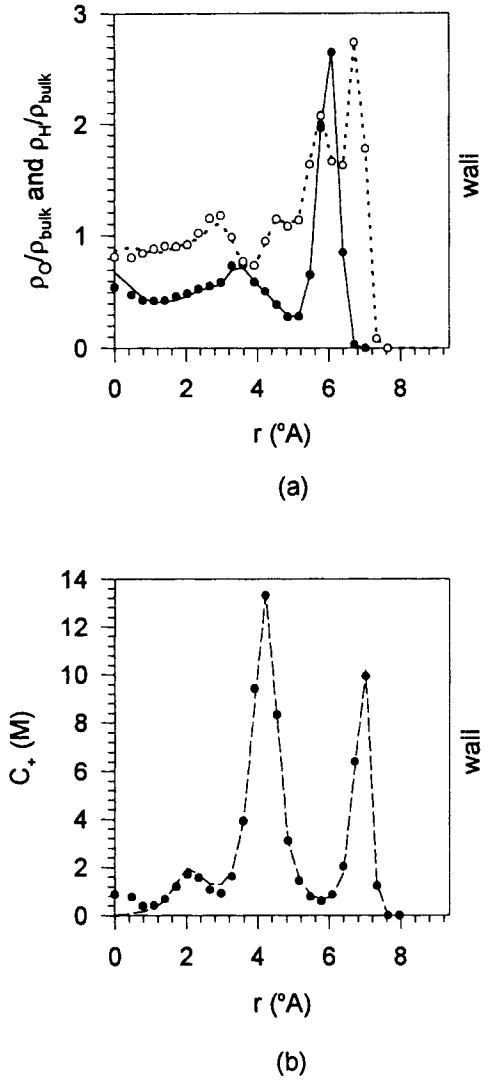

Figure 4. Water and protons in the small pore (cases 3 and 4).

$q_w = -0.1083$ C/m^2. (a) Water distributions: solid line: oxygen atoms in case 3; dotted line: hydrogen atoms in case 3; solid dots and open dots: oxygen and hydrogen atoms in case 4. (b) Proton distribution: dashed line: case 3; solid dots: case 4.

shown in Figure 5a. These peak densities are close to the values shown in case 4, while the water density in the pore center is close to that of the bulk water. However, in Figure 5b, the first peak of the protons becomes even smaller and the second peak becomes much larger. A third peak is also evident. This supports the hypothesis of proton hydration. With the higher number of water molecules in the pore, most of the protons are strongly hydrated to water molecules and are not free to contact the wall directly.

The basic features of the water distributions in the larger pore, which are shown in Figure 6a, are similar to the distributions in the small pores. The proton distributions, shown in Figure 6b, also reveal that most of the protons are strongly hydrated. The concentration of protons demonstrates distinct oscillatory behavior and that some protons move from the wall toward the center of the pore.

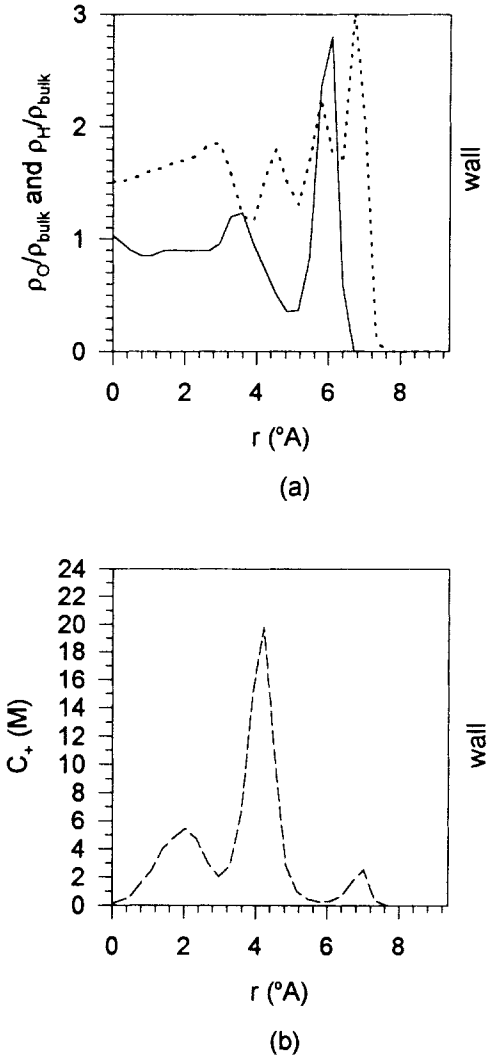

Figure 5. Water and protons in the small pore (case 5).

$q_w = -0.1083$ C/m^2. (a) Water distributions: solid line: oxygen atoms; dotted line: hydrogen atoms. (b) Proton distributions.

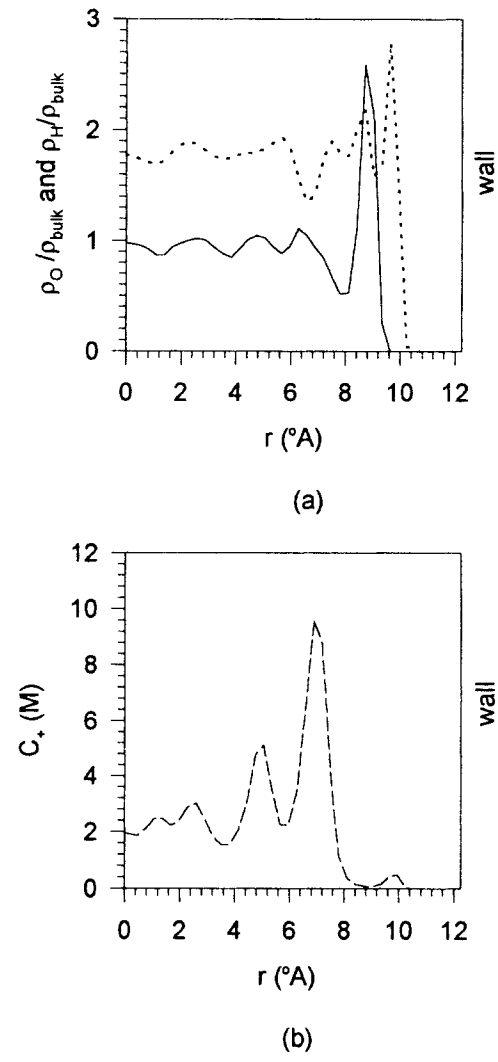

Figure 6. Water and protons in the large pore (case 9).

$q_w = -0.1012$ C/m^2. (a) Water distributions: solid line: oxygen atoms; dotted line: hydrogen atoms. (b) Proton distributions.

Negatively charged pores at q_w-0.2 C/m^2

Cases 6, 7 and 10 (Table 2) correspond to wall charge densities of -0.2 C/m^2. In case 6, the water content is very low. The results for this case are shown in Figures 7a and 7b. Figure 7a shows that almost all the water molecules are attracted to the wall, and Figure 7b shows that all the protons are attracted to a single layer close to the wall, which is about 2.02 Å away from the wall atoms. There is one oxygen density peak, but there are two hydrogen density peaks. This indicates that the hydrogen atoms are located at the two sides of the oxygen atoms. The distances between these peaks and the wall atoms are, respectively, 3.27 Å for the oxygen atoms, 2.34 Å and 3.59 Å for the hydrogen atoms.

With a higher number of water molecules than case 7, water distributes itself throughout the pore, as shown in Figure 8a. Compared to the water distributions at the weaker wall charge density of Figure 5, the density peaks of the oxygen and hydrogen atoms, shown in Figure 8a, are higher. The proton distribution in Figure 8b still shows a sharp peak close to the wall. In addition, we observe a second, very small peak, at about 3.12 Å from the first one. Between the two peaks, there are almost no protons. This implies that those protons, that are not in contact with the wall are strongly hydrated. The same phenomenon is also observed in the simulations for the larger pore, which are shown in Figure 9. Therefore, the wall atoms and the protons in the contact layer together behave like a weakly charged wall.

In the cases 5, 7, 9 and 10 (Table 2) the water densities in the central region of the pores are close to the bulk water density. Therefore, the pores in these four cases may be considered as fully hydrated. For these pores the two layers of water molecules near the walls are strongly affected by the protons.

Other MD simulations were also performed to study the absorption of ions from aqueous media onto charged walls (Glosli and Philpott, 1992, 1993; Rose and Benjamin, 1993). In these studies, water molecules and ions are bound by two parallel slabs, and the wall charge is generally weaker than

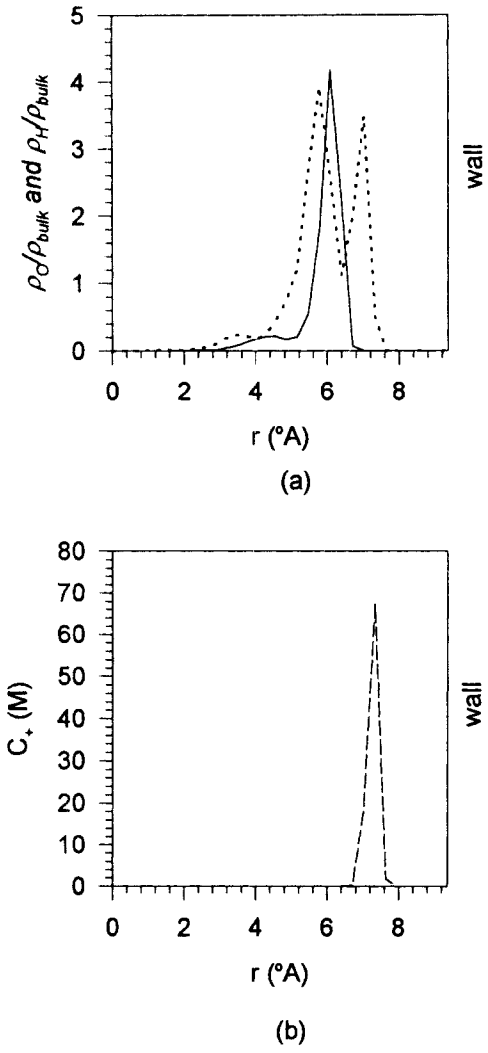

Figure 7. Water and protons in the small pore (case 6).

$q_w = -0.2046$ C/m^2. (a) Water distributions: solid line: oxygen atoms; dotted line: hydrogen atoms. (b) Proton distributions.

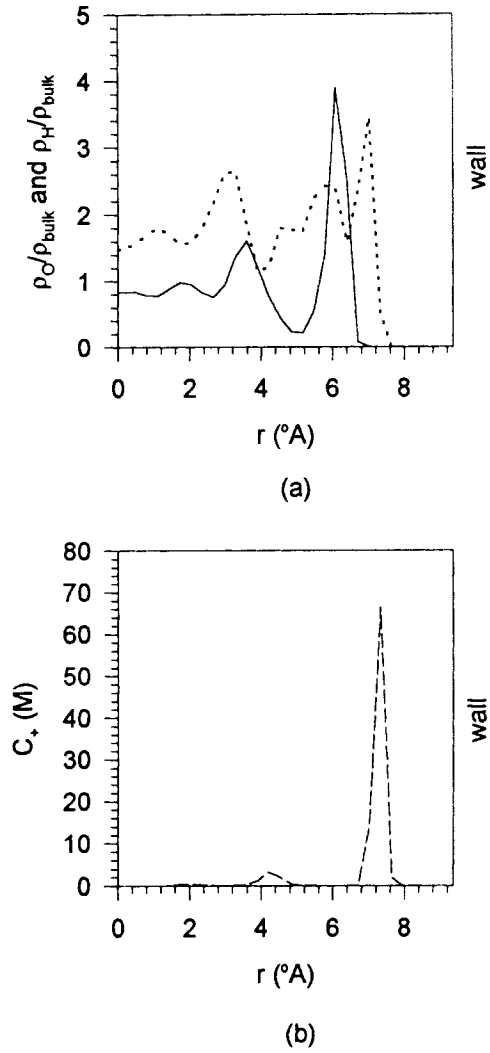

Figure 8. Water and protons in the small pore (case 7).

$q_w = -0.2046$ C/m^2. (a) Water distributions: solid line: oxygen atoms; dotted line: hydrogen atoms. (b) Proton distributions.

-0.1 C/m^2. They found that the ion sizes play an important role in determining the microscopic structure of ions near walls. Small ions are strongly hydrated to water molecules, which separate ions from the wall, whereas large ions favor direct contact with the wall. Since only one pair of ions (one cation and one anion) is simulated in these studies, the oscillation of ion distributions is not observed in the simulations. The results of the present work show that, if the wall charge density is -0.1 C/m^2, the protons are strongly hydrated to water molecules and are not in direct contact with the wall whereas, if the wall charge density is -0.2 C/m^2, most of the protons are absorbed by the wall.

Velocity distributions in electroosmotic flows

From the MD simulations we obtained the velocity distributions of water and protons in the pores, which are shown in Figures 10 and 11. The average velocity of the protons in both figures is $0.1V_0$. It must be pointed out that the noise-to-signal ratio was very large. Because of this it was impossible to obtain a smooth distribution, especially at the low-density locations. However, some qualitative conclusions can still be obtained from the results:

1. In all the cases considered, both water and protons demonstrate high slip velocities at the walls. This indicates that the friction between the water and the walls, or between protons and the walls, is very small. Therefore, for electrolyte solutions in these pores, the no-slip condition is not valid.

2. At $q_w - 0.1$ C/m^2, the velocity distributions of water and protons are close to the average velocity $0.1\ V_0$.

3. At $q_w - 0.2$ C/m^2, water velocities in the pores are still close to the average velocity, whereas proton velocities increase roughly linearly from the walls. The velocity profiles of protons in Figure 10b and 11b appear discontinuous, because no protons were observed at several sections of the pore.

Comparison with experimental results

From the simulation results, we calculated the electroosmotic drag coefficients, average current densities, electric

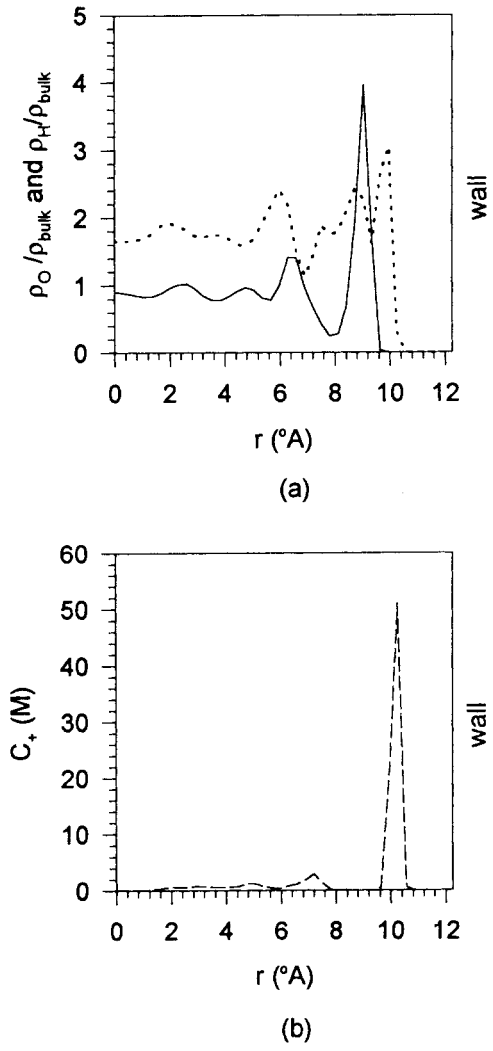

Figure 9. Water and protons in the large pore (case 10).

$q_w = -0.2024$ C/m^2. (a) Water distributions: solid line: oxygen atoms; dotted line: hydrogen atoms. (b) Proton distributions.

fields, specific conductances, ionic mobilities, and proton diffusion coefficients. The results are listed in Table 3 for cases 5, 7, 9 and 10 (these cases are considered as fully hydrated). Experiments (Zawodzinski et al., 1993a) reveal that, for the Nafion-117 membrane in equilibrium with liquid water, the water content must be about 22. Apparently the water content in case 9 is close to this value. The requirement for the water content in the pore is satisfied in the case of a wall charge density stronger than -0.1 C/m^2, if the pores in the membrane are larger than the pore in case 9. In the case of wall charge density lower than -0.1 C/m^2, this requirement is satisified if the pores in the membrane are smaller than the pore of case 9.

In all the cases considered here, the values of ξ are slightly smaller than the theoretical maximum values, that is, β. For the fully hydrated Nafion-117 membrane, 2.5 water molecules being dragged across the membrane per proton is reported (Zawodzinski et al., 1993a). This value is much smaller than the MD simulations of cases 5, 7, 9, and 10. This discrepancy may be due to the complex structures of the real membrane, which significantly restrict the water flow in actual pores. For example, in practical membranes, the wall charges are present in ionic groups instead of being uniformly distributed and the pores exhibit considerable tortuosity, instead of being straight. It must also be pointed out that there are no direct measurements of the pore charge density of Nafion membranes. The pore charge density of these membranes has been indirectly calculated to be in the range from -0.1 to -0.8 C/m^2, depending on the external conditions. The present study supports the lower values of the wall charge density.

Since the average velocity of protons is forced to be $0.1V_0$ in the electroosmotic flows, the average current in the pore is proportional to the proton number. Therefore, in Table 3, the stronger wall charge density (cases 7 and 10) leads to larger current. At the stronger wall charge density, most of the protons are attracted to the walls, and the friction between the protons and the walls increases. This case needs a higher electric field to maintain proton flow, as shown in

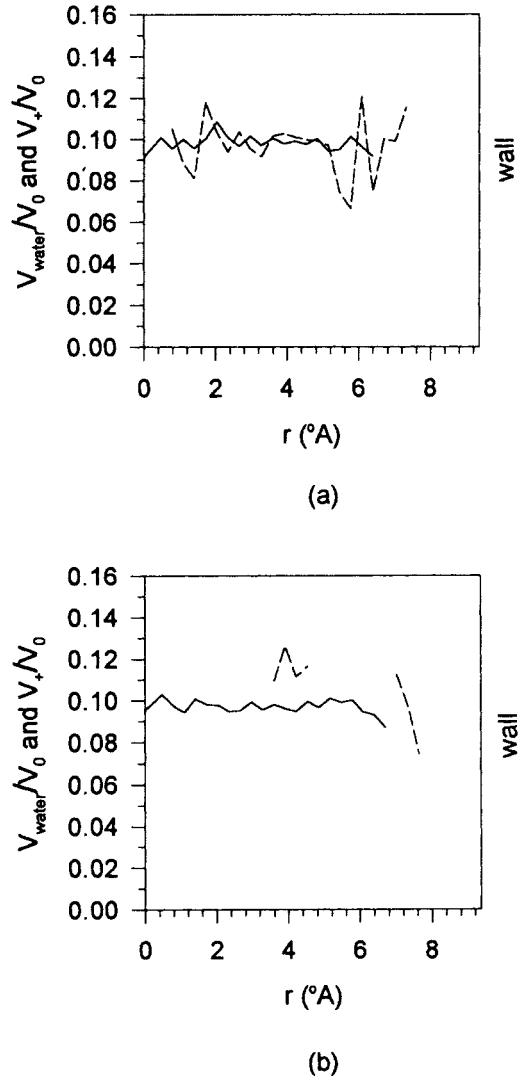

Figure 10. Velocity distributions in the small pore.

(a) Case 5, $q_w = -0.1083$ C/m^2. (b) Case 6, $q_w = -0.2046$ C/m^2.

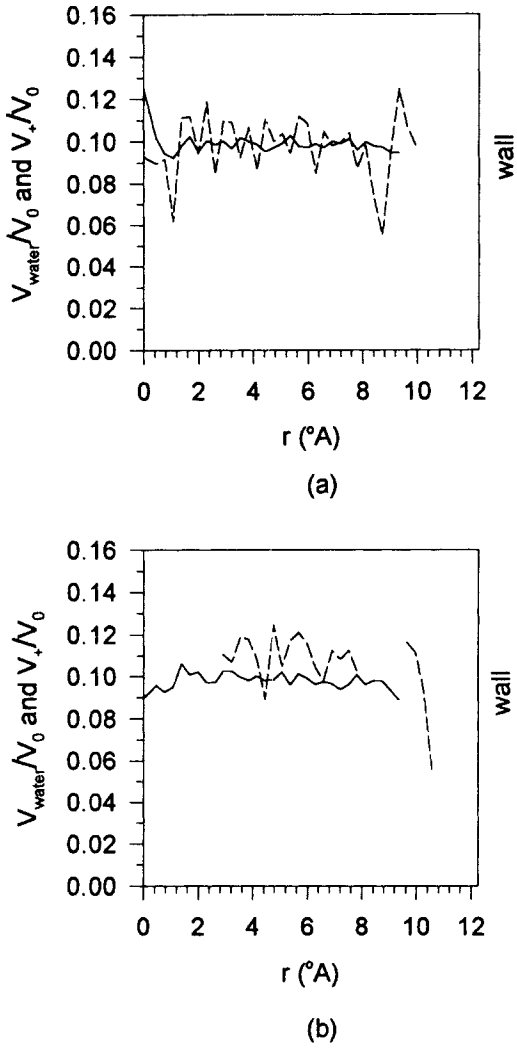

Figure 11. Velocity distributions in the large pore.

(a) Case 9, $q_w = -0.1012$ C/m^2. (b) Case 10, $q_w = -0.2024$ C/m^2.

Table 3. For the same reason, the electric conductance decreases as the wall charge increases.

For the fully hydrated membrane, the conductance from the experiments (Zawodzinski et al., 1993a) is about 0.1 S/cm. As shown in Table 3, at $q_w -0.1$ C/m^2, κ_m of the fully hydrated pores (cases 5 and 9) overestimates the conductance. At $q_w -0.2$ C/m^2, κ_m of the small pore (case 7) matches the experimental value well, whereas κ_m of the larger pore (case 10) underestimates the conductance.

Table 3. Transport Properties of the Membrane Resulting from the Simulations

Case	β	ξ	$\bar{i}$	E	κ	κ_m	u_+	D_+	D_m
5	12.2	12.0	1.917	0.592	3.24	0.350	86.0	22.1	2.39
7	7.65	7.34	3.621	3.681	0.98	0.106	13.8	3.55	0.38
9	20.0	19.6	1.208	0.631	1.91	0.206	80.7	20.7	2.24
10	10.9	10.5	2.417	3.809	0.63	0.068	13.4	3.43	0.37

$\bar{i}$ is the average current in the pore in 10^6 A/cm^2; E is the electric field in 10^6 V/cm; κ and κ_m are the specific conductances of the pore and of the membrane, both in S/cm; u_+ is the proton mobility in 10^{-4} cm^2/Vs; and D_+ and D_m are the proton diffusion coefficients in the pore and in the membrane, both in 10^{-5} cm^2/s.

As the wall charge density increases, the proton mobility is greatly reduced. At the same wall charge density, the mobilities in different pores are very close to each other. The proton diffusion coefficient varies in an analogous way to the mobility. In a free solution at infinite dilution, the proton diffusion coefficient is $D_{+\text{bulk}} = 9.312 \times 10^{-5}$ cm^2/s (Newman, 1973). In the MD simulations at $q_w -0.2$ C/m^2 (cases 7 and 10), D_+ are much smaller than $D_{+\text{bulk}}$, because of the strong friction between the wall and the protons. At $q_w -0.1$ C/m^2 (cases 5 and 9), values for D_+ are more than twice that of $D_{+\text{bulk}}$. This overestimation is mainly caused by the large movement of water in the pores, which reduces the resistance between water and protons. Therefore, the diffusion coefficients, calculated by the Nernst–Einstein equation, are larger than $D_{+\text{bulk}}$. In general, the proton diffusion coefficient in the membrane is about an order of magnitude less than $D_{+\text{bulk}}$ (Verbrugge and Hill, 1990c). In Table 3, the values of D_m are all significantly smaller than $D_{+\text{bulk}}$. For the Nafion-117 membrane, the proton diffusion coefficient obtained from experiments (Verbrugge and Hill, 1990d) is about 1.4×10^{-5} cm^2/s. In Table 3, at $q_w -0.2$ C/m^2 (cases 7 and 10), D_m is less than 0.4×10^{-5} cm^2/s; at $q_w -0.1$ C/m^2 (cases 5 and 9), D_m is larger than 2.1×10^{-5} cm^2/s.

If the Nafion-117 membrane is modeled as a large number of identical cylindrical pores, the wall charge density cannot be as strong as -0.2 C/m^2, because at this wall charge density, κ_m and D_m (as obtained from the simulations) will generally underestimate the proton diffusion coefficient in the membrane and the membrane conductance. At the lower wall charge density, the distortion of the κ_m and D_m values in the simulations is mainly caused by the high value of the thermal motion of water in the pore. If one controlled the electroosmotic drag coefficient to values close to those obtained in the experiments and then calculated values for κ_m and D_m, the latter would be very close to the corresponding experimental values. Therefore, the effective wall charge of the pores in the Nafion-117 membrane is probably closer to he low wall charge density.

Comparison with the Poisson–Boltzmann theory

We used the Poisson–Boltzmann theory to study the cation distributions in a small pore and a large pore. The pore radii were chosen as the actual radii occupied by the solutions in the pores used in the MD simulations. The wall was negatively charged and the charge density was $q_w = -0.1$ C/m^2 or -0.2 C/m^2. The two pores correspond to the models used in cases 5, 7, 9 and 10. The external solution is 1:1 electrolyte and its concentration is 0.1 M or 1 M. The effective ion radius is 4.5 Å. This includes the collective effect of ion and solvent hydration.

The cation distributions in the pores, under different wall charges and external concentrations, are shown in Figures 12 and 13. In all the cases considered here, the distributions monotonically increase toward the wall. These distributions strongly deviate from the MD simulations, shown in Figures 6 to 9. Therefore, the Poisson–Boltzmann theory completely fails in predicting the proton distributions in the pores. This is mainly due to the fact that the Poisson–Boltzmann theory

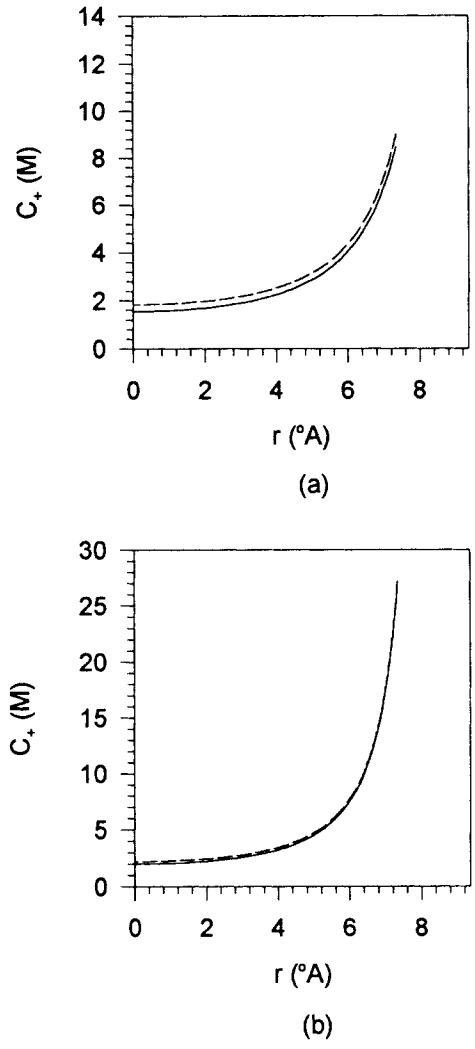

Figure 12. Cation distributions in the small pore.

Solid line: 0.1-M external solution; dashed line: 1-M external solution. (a) $q_w = 0.1$ C/m^2; (b) $q_w = 0.2$ C/m^2.

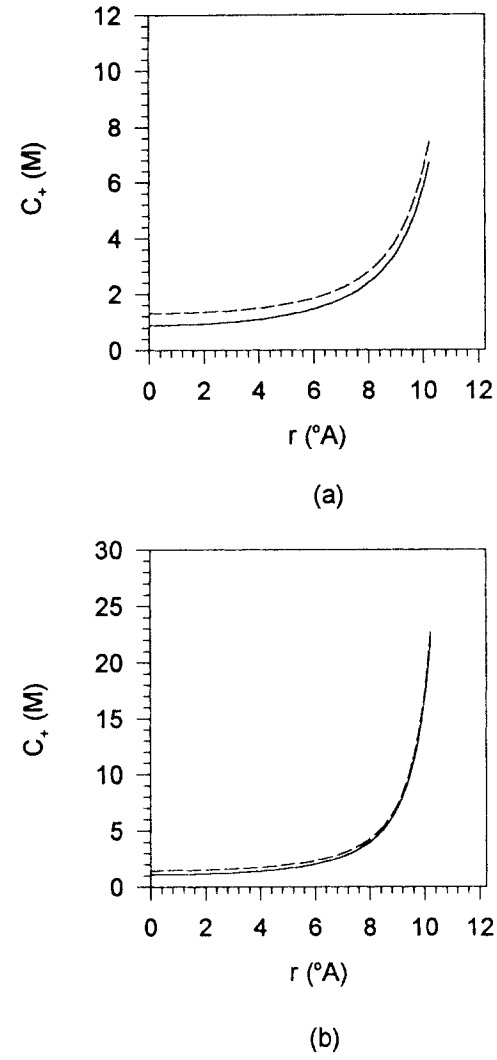

Figure 13. Cation distributions in the large pore.

Solid line: 0.1-M external solution; dashed line: 1-M external solution. (a) $q_w = 0.1$ C/m^2; (b) $q_w = 0.2$ C/m^2.

is based on assumptions that effectively ignore the ion sizes, the ion–ion correlations, and the ion–solvent interactions.

Conclusions

When a solution flows in pores, both water and protons exhibit large slip velocities at the wall. All simulations show that the no-slip condition in continuum hydrodynamics is not valid at the micropore level. Howeer, the flow does not significantly change the water and proton distributions. At the low wall charge density, if the pore is fully hydrated, most of the protons are strongly hydrated too and they do not directly contact the wall. When the wall charge density is high, most of the protons are attracted to the wall. In this case, if the pore is fully hydrated, the absorbed protons and the wall charges together behave like a weakly charged wall. Calculations showed that the classic Poisson–Boltzmann theory fails to predict the proton distributions in the pores.

Compared to the experimental results of the Nafion-117 membrane, the MD simulations overestimate the electroosmotic drag coefficients. This is mainly due to the simplified physical models used. At the low wall charge density, the simulations overestimate the proton diffusivity and pore conductance and, at the high wall charge density, the simulations generally underestimate the proton diffusivity and pore conductance. If a Nafion-117 membrane is modeled as a large number of identical cylindrical pores, in order to fit the membrane conductance and proton diffusion coefficient, the effective wall charge density in the pores should be significantly below -0.2 C/m^2. In actual membrane applications, fixed charge sites exist in ion groups and the wall of the pores is more complex than the ideal models used in this study. These features have important influence on water distributions, ion absorptions, and slip velocities on the wall.

Acknowledgments

Financial support for this research project was provided by NSF and LEQSF to Tulane University, for which the authors are thankful. The authors are also grateful to Dr. Peter N. Pintauro for his valuable advice.

Notation

C_+ = proton concentration
F = Faraday constant
k_B = Boltzmann constant
T = temperature of the system
ρ_{bulk} = water density in bulk solution, 1/18 mol/cm^3

Literature Cited

Berendsen, H. J. C., J. R. Grigera, and T. P. Straatsma, "The Missing Term in Effective Pair Potentials," *J. Phys. Chem.*, **91**, 6269 (1987).

Bontha, J. R., and P. N. Pintauro, "Water Orientation and Ion Solvation Effects during Multicomponent Salt Partitioning in a Nafion Cation Exchange Membrane," *Chem. Eng. Sci.*, **49**, 3835 (1994).

Breslau, B. R., and I. F. Miller, "A Hydrodynamic Model for Electro-Osmosis," *Ind. Eng. Chem. Fundam.*, **10**, 554 (1971).

Capeci, S. W., P. N. Pintauro, and D. N. Bennion, "The Molecular-Level Interpretation of Salt Uptake and Anion Transport in Nafion Membranes," *J. Electrochem. Soc.*, **136**, 2876 (1989).

Christoforou, C. C., G. B. Westermann-Clark, and J. L. Anderson, "The Streaming Potential and Inadequacies of the Helmholtz Equation," *J. Colloid Interf. Sci.*, **106**, 1 (1985).

Din, X.-D., "Study on the Transport Processes of Electrolyte Solutions Through Microscopic Pores by Molecular Dynamics Simulations and Theoretical Analysis," PhD Thesis, Dept. of Mechanical Engineering, Tulane Univ., New Orleans, LA (1996).

Din, X.-D., and E. E. Michaelides, "Calculation of Long-Range Interactions in Molecular Dynamics and Monte-Carlo Simulations," *J. Phys. Chem.*, **101**, 4322 (1997).

Din, X.-D., and E. E. Michaelides, "Molecular Simulation of Particle Flows in Micropores," *Liquid-Solid Flows*-1994, M. C. Roco, D. D. Joseph and E. E. Michaelides, eds., ASME, New York, p. 84 (1994).

Epstein, N., "On Tortuosity and the Tortuosity Factor in Flow and Diffusion Through Porous Media," *Chem. Eng. Sci.*, **44**, 777 (1989).

Fair, J. C., and J. F. Osterle, "Reverse Electrodialysis in Charged Capillary Membranes," *J. Chem. Phys.*, **54**, 3307 (1971).

Fuller, T. F., and J. Newman, "Experimental Determination of the Transport Number of Water in Nafion 117 Membrane," *J. Electrochem. Soc.*, **139**, 1332 (1992).

Garcia, A. G. G., P. N. Pintauro, M. W. Verbrugge, and R. F. Hill, "Development of a Space-Charge Transport Model for Ion-Exchange Membranes," *AIChE J.*, **36**, 1061 (1990).

Gierke, T. D., "Cluster Networks in Membrane Pores," *The Electrochemical Society Extended Abstracts*, Vol. 77-2, Atlanta, GA p., 1139 (1977).

Glosli, J. N., and M. R. Philpott, "Molecular Dynamics Simulation of Adsorption of Ions from Aqueous Media onto Charged Electrodes," *J. Chem. Phys.*, **96**, 6962 (1992).

Glosli, J. N., and M. R. Philpott, "Adsorption of Hydrated Halide Ions on Charged Electrodes. Molecular Dynamics Simulation," *J. Chem. Phys.*, **98**, 9995 (1993).

Gross, R. J., and J. F. Osterle, "Membrane Transport Characteristics of Ultrafine Capillaries," *J. Chem. Phys.*, **49**, 228 (1968).

Hoover, W. G., *Computational Statistical Mechanics*, Elsevier, Amsterdam (1991).

Newman, J. S., *Electrochemical Systems*, Prentice Hall, Englewood Cliffs, NJ (1973).

Nguyen, T. V., and R. E. White, "A Water and Heat Management Model for Proton-Exchange-Membrane Fuel Cells," *J. Electrochem. Soc.*, **140**, 2178 (1993).

Rose, D. A., and I. Benjamin, "Adsorption of Na^+ and Cl^- at the Charged-Platinum Interface," *J. Chem. Phys.*, **98**, 2283 (1993).

Ryckaert, J. P., G. Ciccotti, and H. J. C. Berendsen, "Numerical Integration of the Cartesian Equations of Motion of a System with Constraints: Molecular Dynamics of *n*-Alkanes," *J. Comput. Phys.*, **23**, 327 (1977).

Sasidhar, V., and E. Ruckenstein, "Electrolyte Osmosis Through Capillaries," *J. Colloid Interface Sci.*, **82**, 439 (1981).

Van Gunsteren, W. F. V., and H. J. C. Berendsen, "Algorithms for Macromolecular Dynamics and Constraint Dynamics," *Mol. Phys.*, **34**, 1311 (1977).

Verbrugge, M. W., and R. F. Hill, "Ion and Solvent Transport in Ion-Exchange Membranes: I. A Macrohomogeneous Mathematical Model," *J. Electrochem. Soc.*, **137**, 886 (1990a).

Verbrugge, M. W., and R. F. Hill, "Ion and Solvent Transport in Ion-Exchange Membranes: II. A Ratiotracer Study of the Sulfuric-Acid, Nafion 117 Systems." *J. Electrochem. Soc.*, **137**, 893 (1990*b*).

Verbrugge, M. W., and R. F. Hill, "Transport Phenomena in Perfluorosulfonic Acid Membranes during the Passage of Current," *J. Electrochem. Soc.*, **137**, 1131 (1990c).

Verbrugge, M. W., and Hill, R. F., "Analysis of Promising Perfluorosulfonic Acid Membranes for Fuel-Cell Electrolytes," *J. Electrochem. Soc.*, **137**, 3770 (1990d).

Verlet, L., "Computer 'Experiments' on Classical Fluids. I. Thermodynamical Properties of Lennard-Jones Molecules," *Phys. Rev.*, **159**, 98 (1967).

Xie, G., and T. Okada, "Water Transport Behavior in Nafion 117 Membranes," *J. Electrochem. Soc.*, **142**, 3057 (1995).

Yeo, R. S., and J. McBreen, "Transport Properties of Nafion Membranes in Electrochemically Regenerative Hydrogen/Halogen Cells," *J. Electrochem. Soc.*, **126**, 1682 (1979).

Zawodzinski, T. A. J., C. Derouin, S. Radzinski, R. J. Sherman, V. T. Smith, T. E. Springer and S. Gottesfeld, "Water Uptake by and Transport Through Nafion-117 Membranes," *J. Electrochem. Soc.*, **140**, 1041 (1993a).

Zawodzinski, T. A. J., T. E. Springer, J. Davey, R. Jestel, C. Lopez, J. Valerio, and S. Gottesfeld, "A Comparative Study of Water Uptake by and Transport Through Ionomeric Fuel Cell Membranes," *J. Electrochem. Soc.*, **140**, 1981 (1993b).

Zawodzinski, T. A. J., M. Neeman, L. O. Sillerud, and S. Gottesfeld, "Determination of Water Diffusion Coefficients in Perfluorosulfonate Ionomeric Membranes," *J. Phys. Chem.*, **95**, 6040 (1991).

Zhu, S. B., and G. W. Robinson, "Structure and Dynamics of Liquid Water Between Plates," *J. Chem. Phys.*, **94**, 1403 (1991).

Manuscript received Apr. 11, 1997, and revision received Sept. 5, 1997.